

Article

The Mineralogy, Geochemistry and Origin of the Supergene Manganese Occurrences in the Southern Minas Gerais, Brazil

Davi Diorio Parrotti, Fabiano Tomazini da Conceição *  and Guillermo Rafael Beltran Navarro

Instituto de Geociências e Ciências Exatas (IGCE)/Rio Claro (SP), UNESP—Universidade Estadual Paulista, Rio Claro 13506-900, Brazil; davi.parrotti@unesp.br (D.D.P.); guillermo.navarro@unesp.br (G.R.B.N.)

* Correspondence: fabiano.tomazini@unesp.br

Abstract: In equatorial and tropical regions, supergene mineral deposits created during water/rock interactions are found. Simply put, these supergene deposits are formed through the accumulation of low solubility ions or through the preservation of primary minerals. The supergene manganese (Mn) deposits are examples of the economic importance associated with the chemical weathering processes. In Brazil, the Southern Brasilia Orogen (SBO) was generated during the collision between the Paranapanema Craton and the passive margin of the São Francisco Craton. In the southern Minas Gerais (MG), several supergene Mn occurrences are hosted in the SBO, which were originated during the chemical weathering of gondites belonging to the Amparo Complex. Here, we studied the supergene Mn occurrences in the southern MG, more specifically in the municipalities of Ouro Fino and Careaçú. The MnO contents ranged from 25.50 to 28.40 wt% at Ouro Fino and from 16.80 to 21.20 wt% at Careaçú. These supergene Mn deposits have a diverse mineral assemblage, being composed of spessartine, quartz, Mn-oxides, goethite and kaolinite. The various Mn minerals formed due to spessartine incongruent dissolution were hollandites, cryptomelanes, romanechites, pyrolusites and lithiophorites. Both study areas are relevant for the possible opening of mines for the commercialization of Mn.

Keywords: mining activities; supergene deposits; manganese ore; Southern Brasilia Orogen; chemical weathering; Brazil



Citation: Parrotti, D.D.; da Conceição, F.T.; Navarro, G.R.B. The Mineralogy, Geochemistry and Origin of the Supergene Manganese Occurrences in the Southern Minas Gerais, Brazil. *Minerals* **2023**, *13*, 1216. <https://doi.org/10.3390/min13091216>

Academic Editor: Harald G. Dill

Received: 6 July 2023

Revised: 4 August 2023

Accepted: 13 September 2023

Published: 15 September 2023



Copyright: © 2023 by the authors. Licensee MDPI, Basel, Switzerland. This article is an open access article distributed under the terms and conditions of the Creative Commons Attribution (CC BY) license (<https://creativecommons.org/licenses/by/4.0/>).

1. Introduction

Manganese (Mn) is an element that can occur in nature as oxides, hydroxides, silicates and carbonates, being found in various types of mineral classes [1,2]. Generally, Mn occurs in small proportions in soils as secondary minerals, originated during water/rock–soil interaction [3]. The Mn ore is one of the most essential raw materials for producing metallic alloys, especially combined with iron (Fe) for steel manufacturing. In addition, Mn can also be used in the production of other metal alloys associated with copper (Cu), zinc (Zn), aluminum (Al), titanium (Ti) and lead (Pb), in battery manufacturing and in the chemical industry [4,5].

Mn deposits are classified as hydrothermal, sedimentary or supergene deposits [6], which are the main Mn deposits found in tropical regions [7]. Supergene Mn deposits are associated with pedogenetic processes during the soil formation, reflecting the interactions between the bedrock and the local climate (mainly temperature and rainfall), as well as the vegetation and relief [8,9]. Mn oxides and hydroxides (here called MnOx) are the main secondary minerals forming during water/rock interactions, exhibiting a highly complex and diverse mineralogy [3]. MnOx are typical tunnel or layer structures resulting from the linkage of the MnO₆ octahedra, with high specific surface area and adsorption capacity, allowing the control of metal concentrations associated with soils and sediments in water [10–13].

In 2017, the largest global Mn reserves were described in Brazil (272 Mt—32.3%), South Africa (200 Mt—23.7%), Ukraine (140 Mt—16.6%), Australia (91 Mt—10.8%), India (52 Mt—6.2%),

China (43 Mt—5.1%), Gabon (22 Mt—2.6%) and Ghana (12 Mt—1.4%), totaling 98.8% of the world's total reserves [14]. Regarding Brazil, the average Mn content reaches 32.5%, with Minas Gerais (MG—181.2 Mt), Pará (PA—69.3 Mt), Amapá (AM—9.7 Mt) and Mato Grosso do Sul (MS—7.5 Mt) being the states with the largest national reserves [14]. The Brazilian Mn production in 2021 is concentrated in PA (720,182 t), followed by MG (346,475 t) and MS (271,011 t) [15]. The main companies producing Mn in Brazil are VALE SA (MG and PA), Buritirama Mining SA (PA) and Corumbaense Reunida Mining SA (MS) [16]. In addition, Mn ore is also produced in the states of Ceará (CE), Tocantins (TO) and Goiás (GO) [15].

The Southern Brasilia Orogen (SBO) hosts supergene Mn occurrences in the southeastern São Paulo (SP) and southern MG regions [17], formed during the water/rock interactions of gondites, which are metamorphic rocks composed for quartz and spessartine in similar proportions [18]. However, the mineral evolution, the geochemical constituents, and the origin of the supergene Mn occurrences formation are not well explained in the southern MG, more specifically in the municipalities of Ouro Fino and Careaçú. For this purpose, the characterization of supergene Mn occurrences was carried out through petrographic thin sections, X-ray diffraction and scanning electron microscopy with energy-dispersive spectroscopy (SEM-EDS). Additionally, chemical analyses and mineral chemistry were performed to classify these supergene Mn occurrences and to measure the Mn contents in primary and secondary minerals. Consequently, our results provide new insights into the mineralogy, geochemistry and origin of the supergene Mn occurrences in the SBO.

2. Geological Settings

Southeastern Brazil is characterized by the occurrence of several geotectonic units [19]. The Mantiqueira and Tocantins orogenic systems and a portion of the São Francisco Craton are the main geological structures in the area (Figure 1a). The Tocantins Orogenic Belt is formed by the following tectonic units: the Goiás Massif, Brasília Belt, Goiás Magmatic Arc and Paraguay-Araguaia Belt [20,21]. Its geodynamic evolution is associated with convergence events, called the Brasiliano Cycle, subdivided into Brasiliano I (900–700 Ma), Brasiliano II (670–530 Ma) and Brasiliano III (580–490 Ma) [22–25]. The Southern Brasilia Orogen (SBO) was generated during the collision between the Paranapanema Craton and the passive margin of the São Francisco Craton (630 Ma), giving rise to nappes exhibiting SW dipping and transport in an E–W direction [22–25].

In the study areas, the SBO is basically composed of Neoproterozoic rocks that belong to the Socorro–Guaxupé Nappe (SGN) and SBO basement (Itapira Group, Amparo/Serra Negra Complex and Pouso Alegre Complex) (Figure 1b). The SGN constitutes a series of nappes that represent a collisional process, representing a complex terrain of high-grade metamorphic rocks and a wide variety of granites [25–29]. Janasi et al. [30] subdivided the SGN into two segments (Guaxupé Nappe to the north and the Socorro Nappe to the south) by the NE–SW-trending Ouro Fino shear zone, and the area exhibits a dextral and transpressive nature. Rocha et al. 2017 [31] proposed a long-lived metamorphism event from 630 to 600 Ma, with a UHT peak at 630–625 Ma (12 kbar and ~1030 °C).

The SBO basement emerged due to the erosional processes that removed overlying rocks and was subsequently uplifted due to the activity of the Ouro Fino Shear Belt [30,32,33]. The infracrustal rocks of the Amparo Complex, along with the supracrustal rocks of the Itapira Group, constitute an elongated belt known as the Itapira/Amparo, exhibiting a NE–SW orientation, and located between the Guaxupé and Socorro complexes, which form the SGN [33]. The Itapira Group was defined by Ebert [34] as a group of rocks with synchronous ages that are accommodated within special synforms between antiforms composed of older lithotypes from the Amparo Complex. This group underwent regional metamorphism in the medium- to high-grade amphibolite facies, involving partial melting of less refractory rocks and the injection of acidic material [33]. The Amparo Complex, of Transamazonian age, is predominantly a metasedimentary unit, represented mainly by biotite and/or hornblende gneisses, with a predominance of plagioclase feldspar and subordinately garnet, diopside or sillimanite [30]. The Pouso Alegre Complex consists

of rocks composed predominantly of layered orthogneisses, in amphibolite metamorphic facies and with tonalitic to granodiorite composition, where layers and boudins of mafic rocks occur [35].

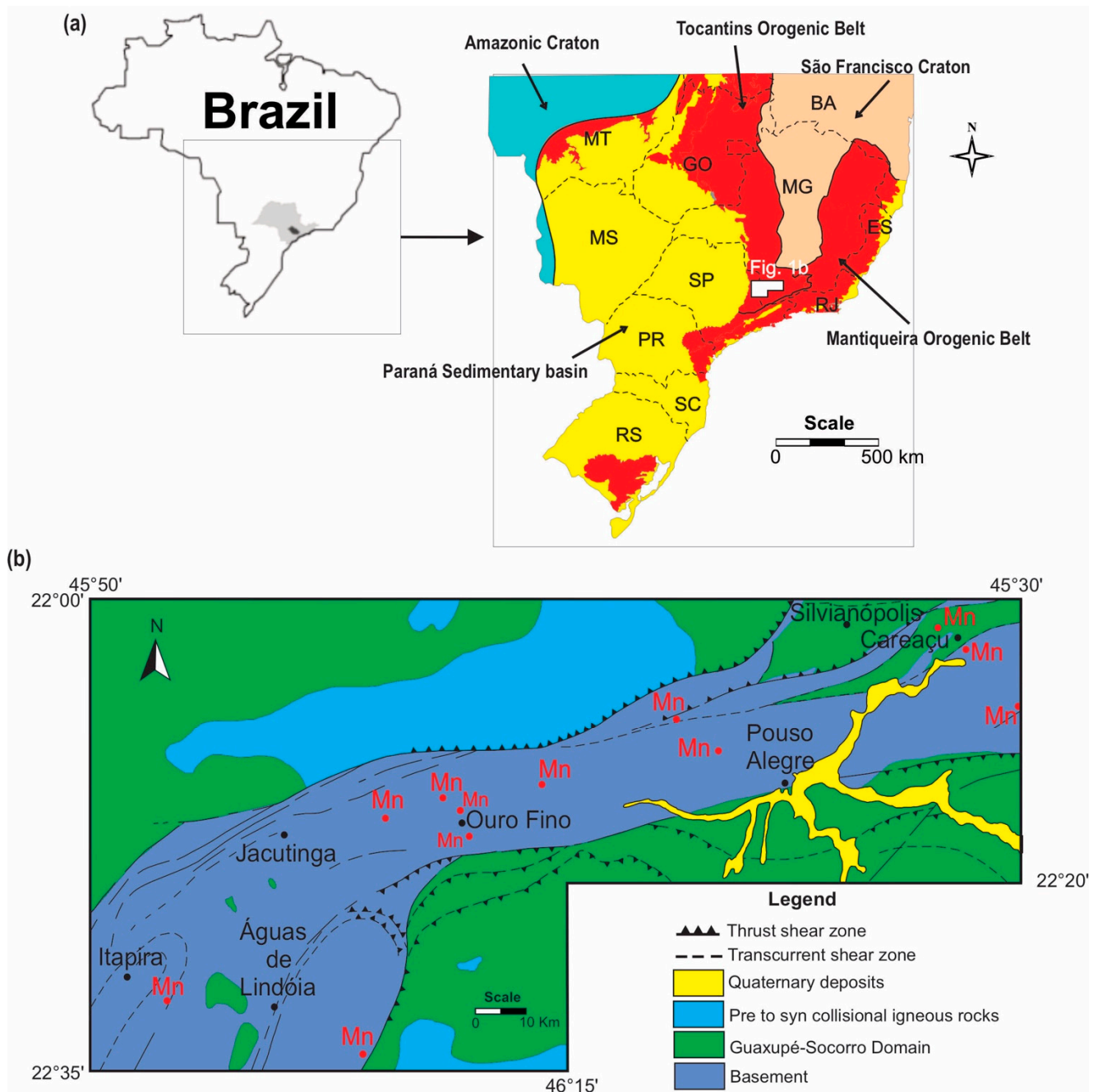


Figure 1. Map of eastern South America showing the main geological units relative to the Cratons, Orogenic Belts and Paraná Sedimentary Basin (modified from Hasui [19]) (a). MT, MS, RS, SC, PR, SP, GO, MG, RJ, ES and BA are the states of Mato Grosso, Mato Grosso do Sul, Rio Grande do Sul, Santa Catarina, Paraná, São Paulo, Goiás, Minas Gerais, Rio de Janeiro, Espírito Santo and Bahia, respectively Simplified geological map and supergene manganese occurrences in the southeastern São Paulo and southern MG regions (modified from Veríssimo [17]) (b).

3. Materials and Methods

3.1. Study Areas

The study areas are part of the Itapira Group (Figure 1b), composed of pelitic, psammopelitic, psammitic, grauwackean, arkosic, marl and calc-silicate sequences, with a regional

metamorphism in the medium- to high-grade amphibolite facies [33]. The supergene Mn occurrences were generated during the chemical weathering of gondite rocks [36], which were stretched and fractured due to boudinage processes [17,37]. Gondites, which can be found as fresh or weathered rocks, are characterized by a persistent rhythmic structure, intercalating quartzite and Mn-garnet layers of varying thicknesses [38]. When these rocks undergo weathering, amorphous materials with a black coloration rich in Mn oxides and hydroxides are generated [39]. The southern MG lies in the Atlantic Plateau (AP) geomorphological provinces [40], more specifically in the Brazilian Atlantic Plateau (BAP), characterized by rolling hills [41].

Ultisols and Oxisols, in the USDA nomenclature, are the predominant soils in the SBO, with deeply chemically and mineralogically stratified weathering profiles [41]. The original vegetation was characterized by savanna vegetation [41]. Based on the Köppen classification [42], the climate in the study areas is classified as subtropical (Cwa), with annual average temperatures varying from 20 to 24 °C [43]. The annual average rainfall in the southern MG ranges from 1350 to 1550 mm, with the highest values of rainfall occurring in the summer period (October to March) compared with dry periods (April to September) [44]. In addition, the study areas are located in the upper course of the Mogi-Guaçu River basin, which has an area of 17,460 km² and an extension of 530 km, covering the northeast region of the state of São Paulo and the southeast of Minas Gerais [45].

3.2. Sampling and Analytical Procedures

Representative samples of supergene Mn occurrences were collected from outcrops in four sampling points near the municipalities of Ouro Fino (samples O3 and O10) and Careaçú (samples C1 and C2) (Figure 2). At the sampling points, the supergene Mn occurrences consist of tabular bodies interbedded in the soil derived from the basement rocks, and have a massive structure, with their color ranging from black to dark gray (Figure 2). Petrographic analyses were conducted on polished thin sections of samples using a Zeiss optical microscope, with digital camera Canon Power Shot G5 (model Axioskop 40, Zeiss, Jena, Germany). In order to confirm the minerals identified by optical microscopy, the samples were powdered and analyzed by X-ray diffractometry (XRD), operating at 40 kV and 40 mA, with CuK α radiation (model Empyrean, Malvern Panalytical, Malvern, United Kingdom). The mineralogical identification was performed by the software Highscore Plus (Malvern Panalytical, Malvern, United Kingdom). In addition, the polished thin sections were analyzed by scanning electron microscopy with energy-dispersive spectrometry (SEM-EDS) (model JSM-6010LA, JEOL, Tokyo, Japan), operating using acceleration voltages of 15 kV and beam current of 15 nA.

The geochemical procedures were carried out at SGS Geosol Laboratory (Belo Horizonte, Brazil) and all details on the sample preparation and quality control are outlined by [46]. All samples were analyzed for major oxides (Na₂O, K₂O, MgO, CaO, SiO₂, TiO₂, Al₂O₃, Fe₂O₃, P₂O₅, MnO and BaO) using X-ray fluorescence (modelo Zetium, Malvern Panalytical, Malvern, United Kingdom), with detection limits of 0.10%. Loss on ignition (LOI) was measured by weight difference after combustion at 1000 °C. Selected spessartine and supergene Mn mineral grains underwent electron microprobe analysis (model JXA-8230 Superprobe, JEOL, Tokyo, Japan). The electron microprobe was operated using a beam diameter of 0.5 μ m, acceleration voltages of 15 kV and beam current of 15 nA. Oxygen was measured as an unknown and the following standards were used: KAlSi₃O₈ (K), CaSiO₃ (Ca), NaAlSi₃O₈ (Na and Si), CaMgSi₂O₆ (Mg), Fe₂O₃ (Fe and O), FeTiO₃ (Ti), Al₂O₃ (Al), Ca₅(PO₄)₃(Cl) (P), MnO₂ (Mn) and BaSO₄ (Ba).

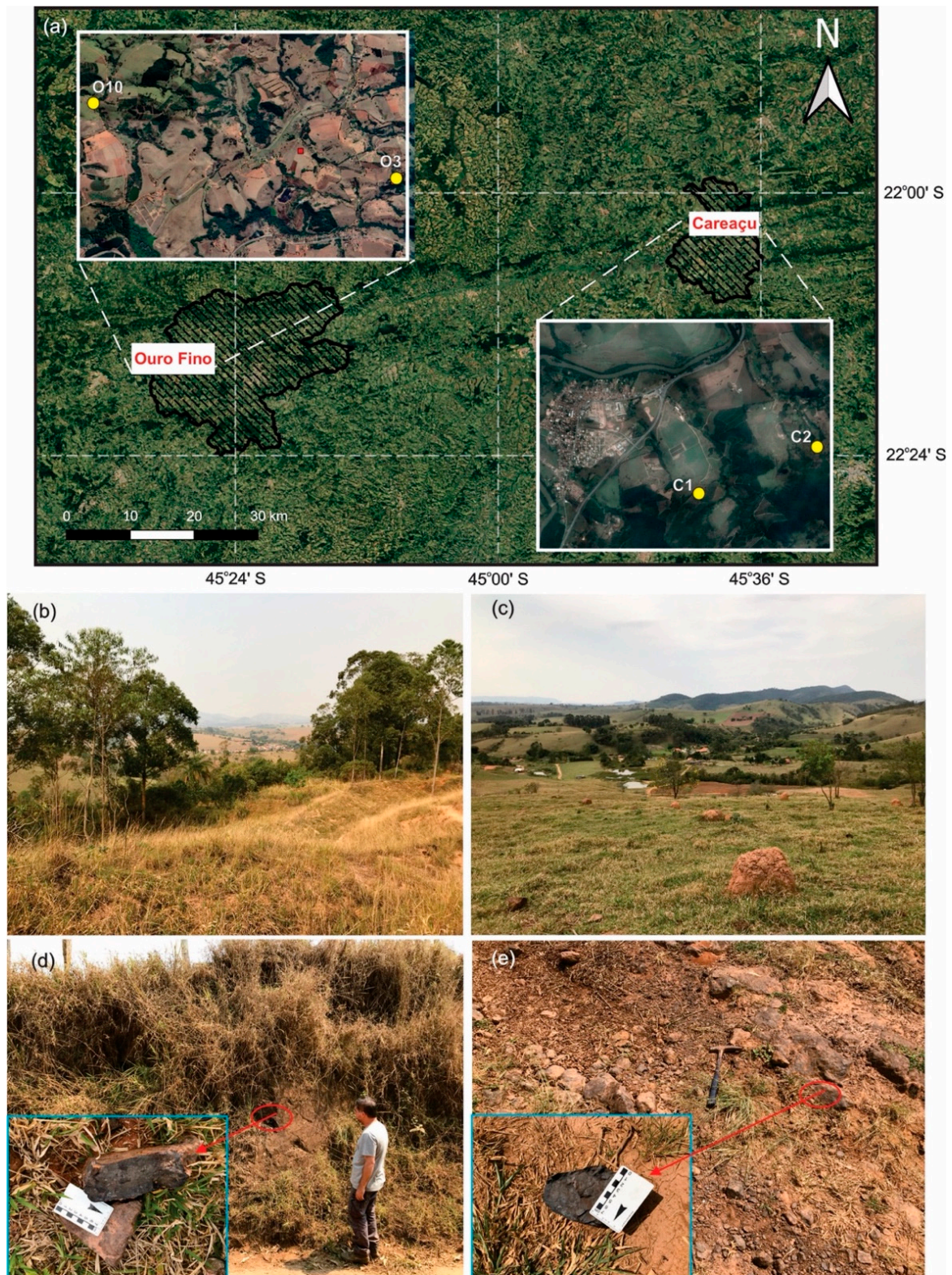


Figure 2. Location of sampling points at Ouro Fino (O3— $22^{\circ}16'06.79''$ S and $46^{\circ}29'45.54''$ W and O10— $22^{\circ}15'30.30''$ S and $46^{\circ}32'22.88''$ W) and Careaçú (C1— $22^{\circ}03'08.60''$ S and $45^{\circ}40'53.40''$ W and C2— $22^{\circ}02'46.90''$ S and $45^{\circ}39'58.87''$ W) (image from Google Earth Pro—June 2021) (a). Landscape overview at sampling points O3 (b) and C2 (c). Outcrops of supergene manganese occurrences where samples O10 (d) and C1 (e) were collected (in detail, the massive structure of supergene manganese, with color black to dark gray).

4. Results

4.1. Petrography

The petrographic analysis revealed a mineral assemblage with a short variation, being composed of primary minerals such as quartz and spessartine, representing ~ 40 and 33%, respectively, followed by Mn-oxides (25%), kaolinite (1%) and goethite (1%) (Figure 3). The XRD patterns confirm the main mineralogy (Figure 4). At Ouro Fino, the grains are equigranular, while at Careaçú, the grains are inequigranular. Ranging from 0.1 to 2.0 mm, the quartz and spessartines grains are anhedral with angular boundaries. Kaolinites and goethite exhibit a maximum dimension of 0.4 mm and occur between the spessartine and quartz.

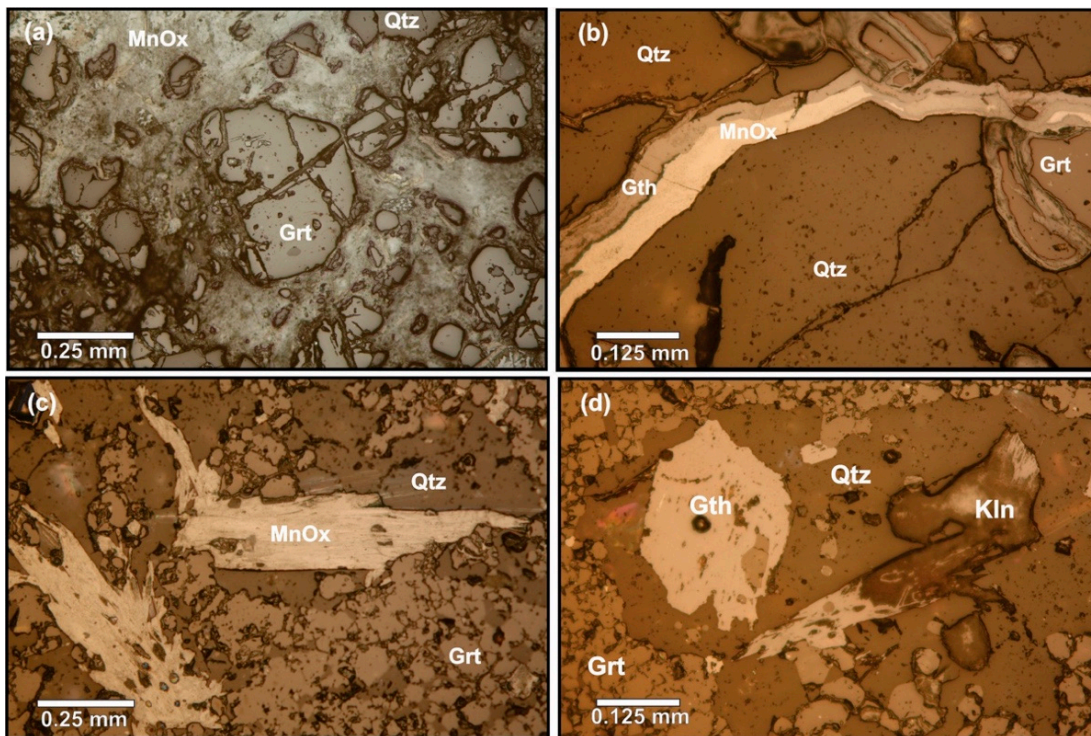


Figure 3. Photomicrographs showing the supergene minerals between the grains of spessartine (Grt) and quartz (Qtz), such as Mn oxides (MnOx) (a–c), goethite (Gth) (b) and kaolinite (Kln) (d). MnOx was used during the petrography, because the optical microscopy does not allow us to identify their different mineral phases.

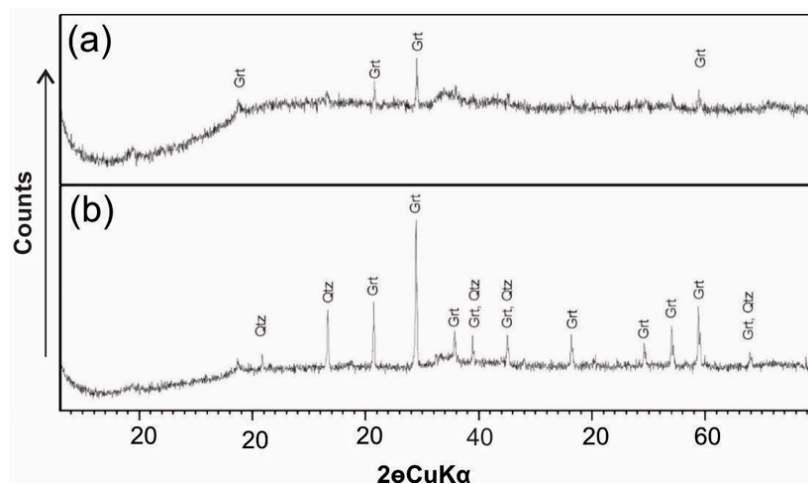


Figure 4. X-ray diffraction (XRD) patterns of supergene manganese occurrences collected at Ouro Fino (sample O10) (a) and Careaçú (sample C1) (b). Spessartine = Grt, quartz = Qtz.

The Mn-oxides observed during petrography share very similar physical characteristics and do not exhibit preferential orientation or significantly different properties among them, not allowing for Mn-oxides identification. Therefore, the Mn-oxides were identified through SEM-EDS analysis, as suggested by Ramdohr [47]. Lithiophorite, cryptomelane, romanechite, hollandite and pyrolusite were the Mn-oxides characterized, with a maximum size of 0.8 mm (Figure 5). These minerals can occur individually but are commonly associated with spessartine.

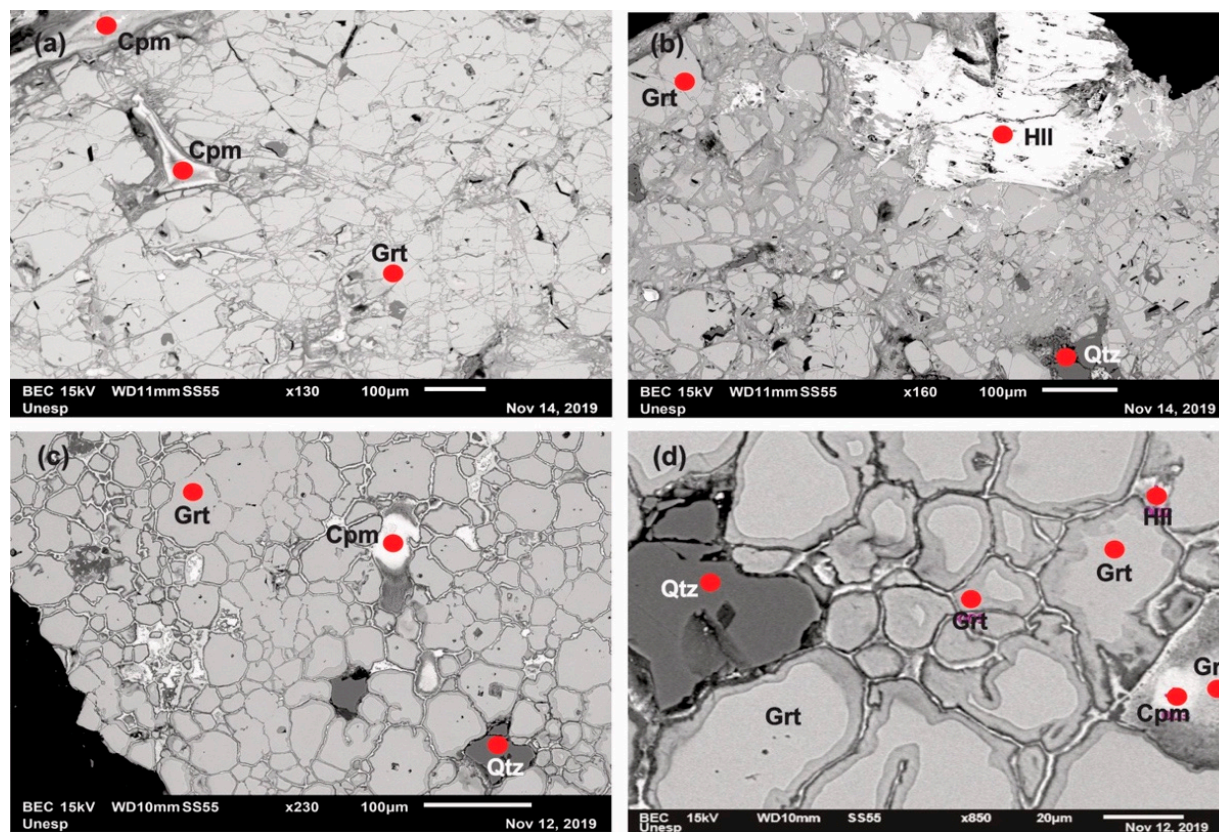


Figure 5. SEM photomicrograph illustrating the supergene manganese occurrences collected at Ouro Fino (sample O3) (a,b) and Careaçú (sample C2) (c,d), with grains of spessartine (Grt), quartz (Qtz), hollandite (Hll) and cryptomelane (Cpm). The red spots were characterized for EDS.

4.2. Chemical Composition

The chemical composition of the supergene Mn occurrences is displayed in Table 1. Table 2 shows the EMPA results for spessartine and Mn-oxides (n = 48 spots).

Table 1. Chemical composition (wt%) of the supergene manganese occurrences in the southern Minas Gerais.

Sample	Na ₂ O	K ₂ O	MgO	CaO	SiO ₂	TiO ₂	Al ₂ O ₃	Fe ₂ O ₃	P ₂ O ₅	MnO	BaO	LOI ¹	Total
Ouro Fino													
O3a	<0.01	0.21	0.22	0.26	36.10	0.53	13.60	5.41	0.10	28.40	0.39	13.49	98.71
O3b	<0.01	0.67	0.16	0.76	35.70	0.47	14.90	6.14	0.19	27.40	0.12	12.03	98.54
O10a	<0.01	0.11	0.29	1.14	39.10	0.28	13.20	6.87	0.13	25.50	0.32	11.42	98.36
O10b	<0.01	0.25	0.45	1.61	38.10	0.61	12.20	7.53	0.15	26.90	0.17	10.89	98.86
Caraçú													
C1a	<0.01	0.07	1.26	5.93	33.20	0.15	18.60	10.40	0.08	19.50	0.04	7.43	97.66
C1b	<0.01	0.19	1.50	3.24	32.50	0.32	19.90	10.21	0.08	21.20	0.13	8.68	97.95
C2a	<0.01	0.08	1.16	4.92	39.60	0.15	16.80	12.20	0.08	16.80	0.12	6.28	98.19
C2b	<0.01	0.06	1.14	4.99	38.30	0.30	16.30	13.19	0.18	17.30	0.07	6.81	98.64

¹ Loss on ignition.

Table 2. Electron microprobe analyses (wt%) for all grains of spessartine and Mn-oxides collected in the southern Minas Gerais.

Sample	Mineral	O	Al	Si	Na	Mg	Ca	Ba	Ti	K	P	Mn	Fe	Total
Ouro Fino														
O3	Spessartine	40.85	10.95	14.58	<0.01	0.55	2.13	<0.01	0.09	0.01	0.01	26.74	3.35	99.26
O3	Spessartine	39.23	10.91	15.95	0.01	0.51	2.17	<0.01	0.11	<0.01	<0.01	27.65	3.30	99.83
O10	Spessartine	40.70	10.50	14.02	0.01	0.52	2.41	<0.01	0.14	<0.01	<0.01	27.63	3.32	99.24
O10	Spessartine	39.90	10.99	15.15	<0.01	0.51	2.13	<0.01	0.15	<0.01	<0.01	27.51	3.39	99.74
O3	Cryptomelane	36.29	0.02	0.58	<0.01	0.05	<0.01	<0.01	<0.01	1.61	0.08	58.98	0.81	98.41
O3	Cryptomelane	35.90	0.35	0.34	<0.01	0.04	<0.01	<0.01	<0.01	1.20	0.09	59.85	0.85	98.63
O10	Cryptomelane	35.72	0.25	0.26	<0.01	0.02	<0.01	<0.01	<0.01	1.84	0.08	59.30	0.82	98.30
O10	Cryptomelane	36.74	0.62	0.39	<0.01	0.03	<0.01	<0.01	<0.01	1.04	0.11	59.26	0.86	99.05
O3	Romanechite	34.78	0.11	0.08	0.02	0.02	0.05	11.09	0.02	0.18	0.38	51.89	0.11	98.72
O3	Romanechite	35.19	0.08	0.08	0.02	0.02	0.06	11.26	0.02	0.17	0.40	51.57	0.07	98.93
O10	Romanechite	35.45	0.09	0.08	0.02	0.01	0.06	11.09	0.02	0.18	0.41	52.24	0.10	99.75
O10	Romanechite	35.42	0.14	0.07	0.02	0.02	0.05	10.65	0.03	0.20	0.36	51.83	0.13	98.91
O3	Hollandite	37.32	0.72	0.05	0.18	0.06	<0.01	3.29	<0.01	3.26	0.11	54.71	0.11	99.81
O3	Hollandite	36.56	0.77	0.06	0.20	0.05	<0.01	3.23	<0.01	3.25	0.11	54.95	0.10	99.29
O10	Hollandite	36.82	0.83	0.06	0.20	0.06	<0.01	3.40	<0.01	3.18	0.11	54.54	0.14	99.35
O10	Hollandite	36.19	0.58	0.06	0.25	0.05	<0.01	3.12	<0.01	3.34	0.10	55.45	0.12	99.27
O3	Pyrolusite	35.83	0.25	0.80	0.01	0.02	0.09	0.17	<0.01	<0.01	<0.01	62.24	0.42	99.83
O3	Pyrolusite	36.06	0.23	0.68	0.01	0.03	0.10	0.21	<0.01	<0.01	<0.01	61.96	0.46	99.74
O10	Pyrolusite	36.12	0.26	0.71	0.01	0.03	0.11	0.15	<0.01	<0.01	<0.01	61.42	0.40	99.21
O10	Pyrolusite	36.23	0.27	0.73	0.01	0.03	0.08	0.20	<0.01	<0.01	<0.01	61.37	0.51	99.43
O3	Lithiophorite	43.00	13.94	0.26	<0.01	0.04	0.04	0.44	0.14	0.05	0.18	35.64	4.51	98.24
O3	Lithiophorite	42.22	14.35	0.28	<0.01	0.05	0.03	0.55	0.16	0.06	0.20	35.97	4.18	98.05
O10	Lithiophorite	41.95	13.40	0.22	0.02	0.04	0.04	0.40	0.01	0.09	0.05	37.04	4.95	98.21
O10	Lithiophorite	42.55	13.64	0.12	0.01	0.03	0.01	0.51	0.00	0.10	0.03	36.84	4.83	98.67
Careaçu														
C1	Spessartine	39.02	11.13	16.45	0.01	0.87	9.67	<0.01	0.04	<0.01	<0.01	19.46	3.12	99.76
C1	Spessartine	38.95	11.06	16.43	0.01	0.85	9.10	0.02	0.04	<0.01	<0.01	20.28	2.92	99.64
C2	Spessartine	39.16	11.04	16.05	0.01	<0.01	9.32	0.01	0.02	<0.01	0.01	19.31	4.21	99.14
C2	Spessartine	39.23	10.76	16.10	0.03	0.03	9.15	0.01	<0.01	0.01	0.01	19.46	4.24	99.03
C1	Cryptomelane	35.81	0.03	0.05	0.12	0.01	<0.01	<0.01	<0.01	2.66	0.19	58.97	0.59	98.43
C1	Cryptomelane	36.70	0.15	0.06	0.13	0.02	<0.01	<0.01	<0.01	2.82	0.19	58.07	0.65	98.79
C2	Cryptomelane	36.91	0.14	0.08	0.17	0.02	<0.01	<0.01	<0.01	2.95	0.24	57.56	0.63	98.70
C2	Cryptomelane	36.60	0.22	0.18	0.07	0.04	<0.01	<0.01	<0.01	2.35	0.17	58.51	0.94	99.08
C1	Hollandite	36.64	0.16	0.11	0.04	0.03	0.09	4.47	<0.01	1.59	0.20	55.23	0.59	99.15
C1	Hollandite	36.01	0.14	0.08	0.17	0.05	0.03	4.99	<0.01	2.66	0.19	54.05	0.65	99.02
C2	Hollandite	36.60	0.22	0.18	0.07	0.02	0.05	4.04	<0.01	2.32	0.24	54.93	0.36	99.03
C2	Hollandite	36.03	0.17	0.11	0.07	0.05	0.03	4.82	<0.01	2.26	0.17	55.29	0.63	99.63
C1	Pyrolusite	35.10	0.21	0.74	0.01	0.03	0.10	0.18	<0.01	<0.01	<0.01	63.06	0.41	99.84
C1	Pyrolusite	35.22	0.24	0.69	0.01	0.02	0.11	0.20	<0.01	<0.01	<0.01	62.88	0.50	99.87
C2	Pyrolusite	34.89	0.22	0.70	0.01	0.03	0.10	0.17	<0.01	<0.01	<0.01	62.63	0.44	99.19
C2	Pyrolusite	35.16	0.23	0.72	0.01	0.02	0.09	0.19	<0.01	<0.01	<0.01	62.91	0.47	99.80
C1	Lithiophorite	45.09	13.21	0.02	0.02	0.01	0.02	0.06	<0.01	0.02	<0.01	38.21	2.07	98.73
C1	Lithiophorite	44.66	12.93	0.08	0.01	0.02	0.02	0.04	<0.01	0.03	<0.01	38.15	2.08	98.02
C2	Lithiophorite	45.82	12.28	0.12	0.01	0.02	0.02	0.01	<0.01	0.06	<0.01	38.01	2.07	98.42
C2	Lithiophorite	45.88	12.42	0.02	0.02	0.02	0.03	0.05	<0.01	0.03	<0.01	37.77	2.10	98.34

The supergene Mn occurrences have elevated SiO₂ and Al₂O₃ contents in relation to the other major oxides, ranging from 35.70 to 39.10 wt% and from 12.20 to 14.90 wt% at Ouro Fino and from 32.50 to 39.60 wt% and from 16.30 to 19.90 wt% at Careaçú, respectively. In the study areas, the MnO content decreases from the Ouro Fino to the Careaçú samples, varying from 25.50 to 28.40 wt% and from 16.80 to 21.20 wt%, respectively. In contrast, the CaO and Fe₂O₃ contents are higher in the samples collected at Careaçú than at Ouro Fino. In addition, LOI contents in the samples collected at Ouro Fino (average of 11.96 wt%) are higher than at Careaçú (average of 7.30 wt%).

Spessartines contain large amounts of Mn (averages of 27.30 wt% at Ouro Fino and 19.63 wt% at Careaçú) and Si (averages of 15.23 wt% at Ouro Fino and 16.26 wt% at Careaçú). The average Fe and Ca contents were 3.35 wt% at Ouro Fino and 3.62 wt% at Careaçú, and 2.14 wt% at Ouro Fino and 9.31 wt% at Careaçú, respectively. The inverse relationship between Mn and (Fe + Ca) (Figure 6a) results from Mn substitution into spessartines, which have the chemical formulae [(Mn_{1.8},Ca_{0.9},Fe_{0.3})Al₂(SiO₄)₃] at Ouro Fino and [(Mn_{2.5},Fe_{0.3},Ca_{0.2})Al₂(SiO₄)₃] at Careaçú.

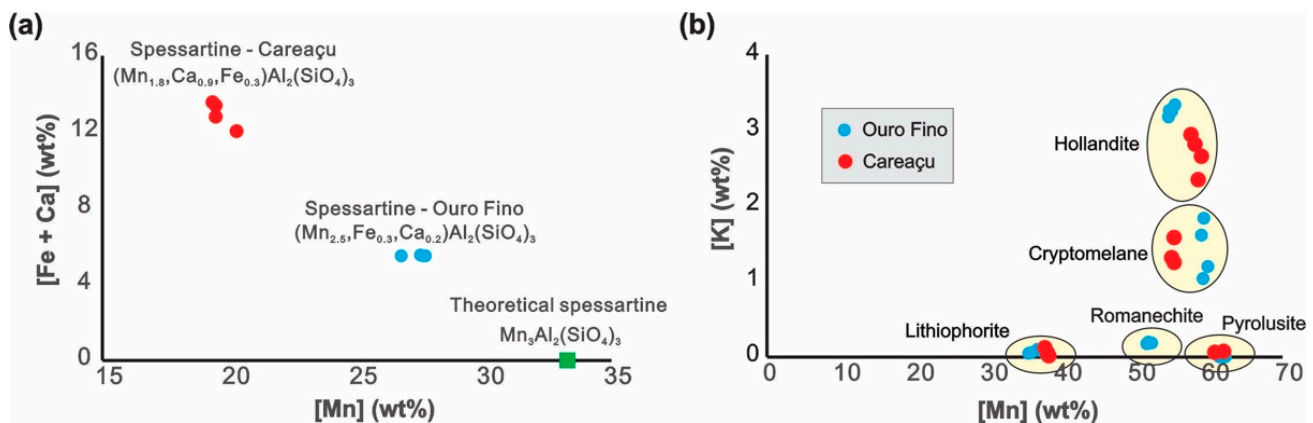


Figure 6. Mn-(Fe + Ca) (a) and Mn-K (b) contents in the supergene manganese occurrences and spessartite, respectively, collected at Ouro Fino and at Careaçú.

Figure 6b illustrates the relationship between Mn and K in Mn-oxides. The EMPA analyses reveal that hollandites contain K averages of 3.25 wt% at Ouro Fino and 2.21 wt% at Careaçú, while the cryptomelanes have K averages of 1.42 wt% at Ouro Fino and 2.69 wt% at Careaçú. Romanechites, pyrolusites and lithiophorites have low average K contents, <0.03, <0.01 and <0.10 wt%, respectively. Romanechite has high Ba (11.02 wt%), while a high Al content (13.83 wt%) identifies lithiophorite bands. The Mn contents vary from ~36 to ~63 wt%, reflecting the various manganese minerals present. With the EMPA results, the chemical formulae are: (a) cryptomelane—K_{0.27}(Mn_{7.66},Fe_{0.11},Al_{0.08},Si_{0.10})O₁₆, romaneechte—(Ba_{0.40},K_{0.02})(Mn_{4.77},Al_{0.02},Si_{0.01})O₁₀, hollandite—(K_{0.63},Ba_{0.18},Na_{0.17})(Mn_{7.54},Al_{0.20},Fe_{0.02},Si_{0.02})O₁₆, pyrolusite—(Mn_{0.97}Si_{0.03})O₂ and lithiophorite—(Al_{0.59},Fe_{0.10})(Mn_{0.93},Si_{0.01})O₂(OH)₂ at Ouro Fino; (b) cryptomelane—K_{0.55}(Mn_{7.68},Fe_{0.09},Al_{0.04},Si_{0.01})O₁₆, hollandite—(K_{0.43},Ba_{0.25},Na_{0.04})(Mn_{7.57},Al_{0.50},Fe_{0.08},Si_{0.03})O₁₆, pyrolusite—(Mn_{0.97}Si_{0.03})O₂ and lithiophorite—(Al_{0.58},Fe_{0.05})(Mn_{1.05})O₂(OH)₂ at Careaçú.

5. Discussion

5.1. Comparison of the Supergene Mn Occurrences in the SBO and Other Brazilian Deposits

Several supergene Mn occurrences outcrop can be found in the SBO, as illustrated in Figure 1b. These occurrences are derived from chemical weathering of gondites. Based on the Mn content, the Mn ore can be classified into three categories: high-grade Mn ore, with Mn contents higher than 35%; ferruginous Mn ore, with Mn contents between 10 and 35%; and manganiferous Fe ore, with Mn contents between 5 and 10% [48]. Among the supergene Mn occurrences in the SBO, the main area studied is the Cocho Stream Mine, located in the municipality of Itapira (São Paulo State), which has an average of 23%

MnO₂, with the main mineralogy composed of cryptomelane (20%), spessartine (20%), lithiophorite (20%), quartz (15%) and pyrolusite (10%) [39]. Our results showed that the supergene Mn occurrences in the Ouro Fino and Careaçú have an average of ~27 and ~20 wt% MnO₂, respectively. Therefore, the supergene Mn occurrences in the SBO are classified as ferruginous Mn ores, indicating their relevance for the possible opening of mines for the commercialization of Mn.

As mentioned previously, Brazil has significant reserves of Mn distributed throughout its territory. However, the main Mn reserves are concentrated in the states of MG, MS and PA. The Morro da Mina Mn deposit is located in the MG and inserted in the Rio das Velhas Supergroup, specifically within the Lafaiete Formation, identified as a volcanic-sedimentary sequence of the greenstone belt type in the Quadrilátero Ferrífero [49]. The Urucum Mn deposit is located in the MS and associated with a sedimentary deposit characterized by Neoproterozoic banded iron formations (BIFs) with primary Mn-oxides hosted in the Santa Cruz Formation [50,51]. The Azul Mn deposit, located in the central-western Carajás Mineral Province (PA), has an Mn ore originated from sedimentary (mainly rhodochrosite) and supergene origins [52]. The Mn contents in these deposits are ~32, 43 and 38% of MnO₂ at the Morro da mina [53], Urucum [54] and Azul [52] Mn deposits, respectively, these values being higher than the Mn contents in the supergene Mn occurrences in the SBO.

The ⁴⁰Ar/³⁹Ar geochronological data for the Azul Mn deposit indicated different chemical weathering episodes ranging from ~70 to ~10 Ma [55,56]. In the Quadrilátero Ferrífero, the ⁴⁰Ar/³⁹Ar geochronological data proposed a prolonged history of weathering between 62 and 14 Ma, with the majority of MnOx precipitated between 51 and 41 Ma [57]. In both areas, the MnOx precipitation peak was at ~47 Ma [56,57]. Urucum was deposited between 800 and 595 Ma, with metamorphism and hydrothermal alteration at ~575–512 Ma, and their summit rocks have been exposed to weathering for at least ~70 Ma [58,59]. Unfortunately, there are no ⁴⁰Ar/³⁹Ar geochronological data for the supergene Mn occurrences in the SBO. Our chemical mineral results indicated a relatively high K content in cryptomelanes and hollandites, associated with their good crystallinity and lack of contaminants contributing to reliable ⁴⁰Ar/³⁹Ar geochronological data, allowing the comparison of MnOx precipitation ages in the SBO with other Mn deposits in Brazil.

5.2. Origin of the Supergene Mn Occurrences

Due to chemical weathering processes, the more soluble ions are moved by the surface waters to the oceans, while the less soluble ions form secondary minerals [60–63]. Parental rocks, climate, biosphere, relief and time play important roles during chemical weathering processes [60,61]. The temperature and runoff are the main parameters controlling the chemical weathering of igneous and metamorphic rocks, but other factors must be considered to explain the water/rock interactions, such as the variations in landforms and landscapes [64–69]. Both study areas have the same geological, climatic and geomorphological settings, as well as savannah vegetation.

Gondites are lenses interbedded in gneisses belonging to the SBO basement. When the basement reached the Earth's surface, the action of meteoric agents started promoting the chemical weathering of these rocks (Figure 7a). Atmospheric reactions ($\text{CO}_2 + \text{H}_2\text{O} \rightarrow \text{H}_2\text{CO}_3 \rightarrow \text{H}^+ + \text{HCO}_3^-$) and oxidation of organic matter in soils ($\text{HCOOH} + 0.5 \text{O}_2 \rightarrow \text{CO}_2 + \text{H}_2\text{O} \rightarrow \text{H}_2\text{CO}_3 \rightarrow \text{H}^+ + \text{HCO}_3^-$) produce carbonic acid, which is the primary reactant driving chemical weathering processes. During the chemical weathering of gneisses, over a sufficient period of time, deep stratified weathering profiles are formed, and the meteoric waters become enriched in alkali and alkali-earth elements (Figure 7b). The elements dissolved in the upper horizons are transported to lower horizons and depending on the local pH-Eh condition, some elements may reprecipitate in secondary minerals within the system. Gondites are essentially composed of quartz and spessartine. During the interaction between gondites and the enriched meteoric water within saprolites, quartz is not weathered due to its low dissolution rates [70] and spessartines have a low chemical weathering rate [71], leading to supergene Mn occurrences (Figure 7c).

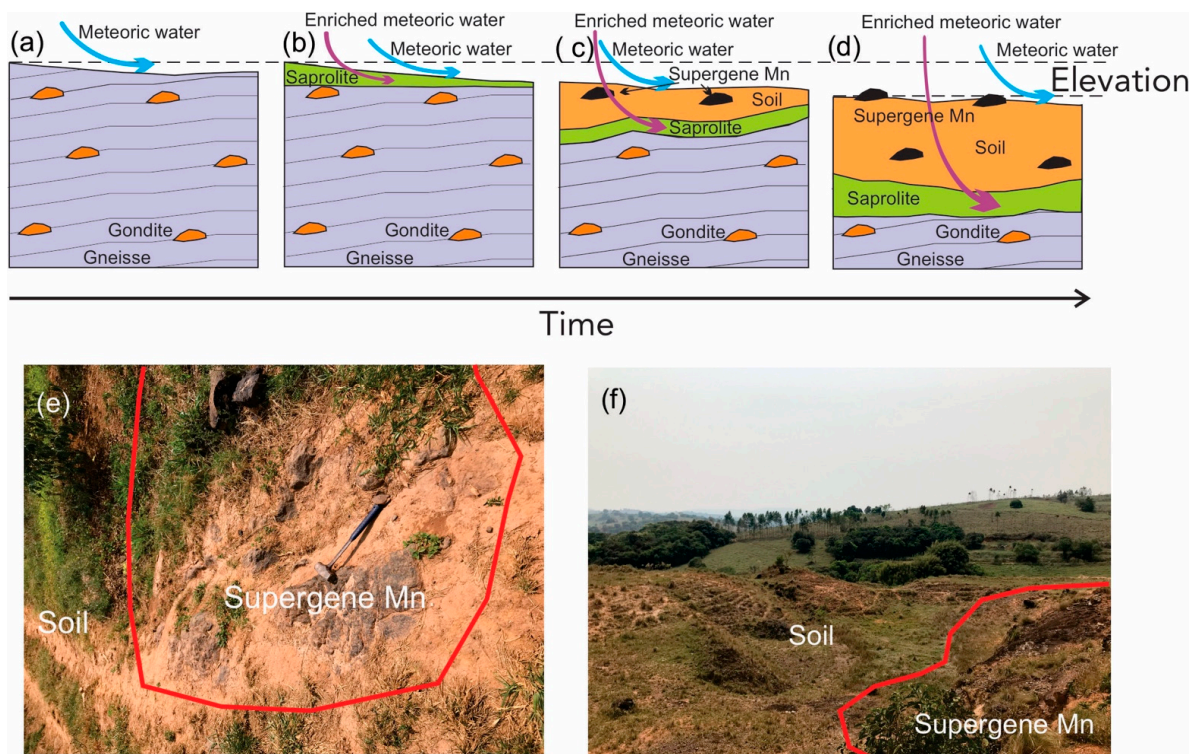
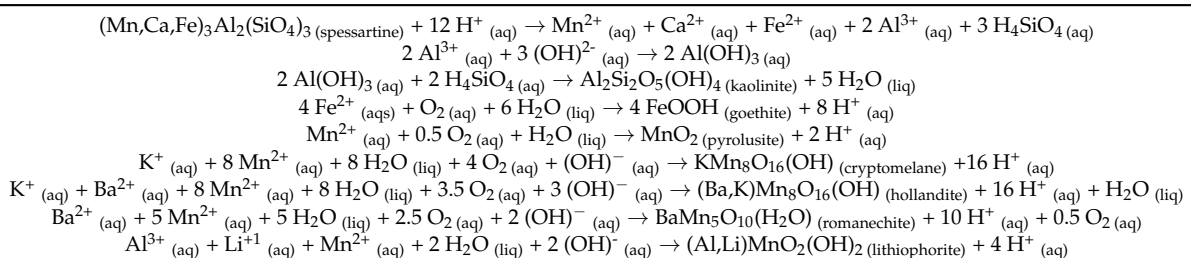


Figure 7. Scheme illustrating the origin of the supergene Mn occurrences in the SBO: the basement reaches the Earth's surface (a); beginning of chemical weathering of gneisses, where meteoric waters enrich in alkaline and alkaline earth elements (b); over a sufficient period of time, a deep stratified weathering profile is formed and the supergene Mn occurrences are originated (c); removal of the upper soil horizons, with the supergene Mn occurrences emerging on the Earth's surface (d). The concomitant presence of soil and supergene Mn occurrences at Careaçu (e) and Ouro Fino (f).

In general, the spessartines are well preserved in the study areas (Figure 4a,c), but their edges exhibit different stages of weathering (Figure 4b,d). The chemical weathering process related to spessartine is the incongruent dissolution, where the Al and SiO₂ released produce kaolinite, Fe forms goethite and Ca is leached into the groundwater. Mn is one of the first elements to be released during the chemical weathering of spessartines, and under oxidizing conditions, the Mn²⁺ changes to Mn³⁺ or Mn⁴⁺ [1,72]. Therefore, most of the supergene Mn minerals formed are formed as Mn⁴⁺, with some Mn³⁺ [3,6]. Mn⁴⁺ forms pyrolusite, while the cryptomelane, hollandite, romanechite and lithiophorite formation results from the recombination of K⁺, Ba²⁺, Al³⁺ and Li⁺ released from the chemical weathering of gneisses and Mn²⁺, Mn³⁺ and Mn⁴⁺ from spessartines. Table 3 summarizes the main chemical weathering reactions associated with spessartines. The petrography and SEM-EDS analyses confirm the chemical weathering processes proposed here.

Table 3. Theoretical chemical weathering reactions showing the most important processes during the interaction between enriched meteoric water and spessartines, originating the supergene Mn occurrences in the SBO.



The presence of kaolinite indicates that the supergene Mn occurrences in SBO are typical deposits formed under the warm and humid tropical paleoclimatic conditions (moderate chemical weathering) found in southeastern Brazil's passive margin. Warm and moderately humid conditions in a savannah-type environment promote active chemical weathering with the advance of the weathering front and low physical erosion, which removes the upper horizons of soils, and the supergene Mn occurrences outcrop at the Earth's surface (Figure 7d). Figure 7e,f illustrate the concomitant outcrops of soil and supergene Mn occurrences. Extensive and systematic future studies involving the $^{40}\text{Ar}/^{39}\text{Ar}$ geochronology, as already carried out in other areas in Brazil [55–59,73–75] and elsewhere [76–82], will provide valuable insights on the weathering history and paleoclimatic conditions during the precipitation of these supergene Mn minerals, as well as on the landscape evolution in the SBO. Likewise, the current climatic conditions also suggest moderate chemical weathering in the study areas, as already proposed for different rock types in southeastern Brazil [83–95]. Recently, Meneguel et al. [96] and Conceição et al. [97] studied the moderate chemical weathering processes to form the raw material used in the porcelain stoneware industry in the São Paulo State and the supergene P, Ti, Nb and REE deposits in the Tapira and Catalão I alkaline-carbonatites complexes, respectively.

The supergene Mn occurrences at Ouro Fino and Careaçú are fine-grained and their mineral phases are difficult to distinguish visually in the field or in hand specimens, as well as in petrography analyses carried out on polished thin sections. Due to their poorly crystalline presentation, the XRD patterns fail to identify the different mineral phases, as also proposed by Ling et al. [98]. Consequently, the SEM-EDS was used here to characterize the Mn-oxides collected at Ouro Fino and Careaçú, even though this technique has experimental limitations [47]. Given the poor crystalline and chemical variability of Mn-Oxides, associated with fine-scale intergrowths of two or more phases, the minerals identified by SEM-EDS should be interpreted carefully. Raman spectroscopy has several advantages for identifying tunnel- or layer-structure Mn-oxides, as well as for investigating changes in response to certain redox, cation-exchange, and other reactions [11,13]. Consequently, future studies using Raman spectroscopy, associated with SEM-EDS and EMPA, will provide unparalleled insights into the micro-mineralogy and chemistry of these complex samples.

6. Conclusions

The supergene Mn occurrences at Ouro Fino and Careaçú are inserted in the SBO basement, and they are found as tabular and massive bodies. The collected samples presented a black color and the petrographic analyses provided important information about the mineralogical composition and physical characteristics of these occurrences. In general, the samples are predominantly equigranular to inequigranular, with a mineral assemblage composed of quartz, spessartine, Mn-oxides, goethite and kaolinite. The MnO contents showed averages of ~27 wt% at Ouro Fino and ~20 wt% at Careaçú, with the supergene Mn occurrences being classified as ferruginous Mn ores, indicating the possibility of opening mines for the commercialization of Mn. The Mn contents in other Mn deposits in Brazil are higher than the Mn contents in the supergene Mn occurrences in the SBO. The dominant meteoric alteration (chemical weathering processes and/or pedogenesis) originates the supergene Mn occurrences, while the physical erosion of the upper horizons of soil is responsible for outcrops of these Mn deposits at the Earth's surface. The Mn contents vary from ~36 to ~63 wt%, reflecting the various manganese minerals. In order to confirm the Mn-oxides, future studies must be carried out using Raman spectroscopy. Finally, the K contents in hollandites and cryptomelanes suggest that these minerals can be used for a reliable $^{40}\text{Ar}/^{39}\text{Ar}$ geochronology, allowing the comparison of MnOx precipitation ages, weathering history, paleoclimatic conditions and landscape evolution in the SBO.

Author Contributions: Conceptualization, D.D.P., F.T.d.C. and G.R.B.N.; methodology, D.D.P., F.T.d.C. and G.R.B.N.; investigation, D.D.P., F.T.d.C. and G.R.B.N.; writing—original draft preparation, D.D.P. and F.T.d.C. All authors have read and agreed to the published version of the manuscript.

Funding: This research was funded by FAPESP (Processes No. 2017/23577-2) and CNPq (Processes No. 307157/2019-9).

Data Availability Statement: Not applicable.

Acknowledgments: The authors thank UNESP for its support during this work. Specially, three anonymous referees and the Associated Editor are thanked for their detailed and insightful review comments, which helped to improve the manuscript.

Conflicts of Interest: The authors declare no conflict of interest.

References

1. Stanton, R.L. *Ore Petrology*, 1st ed.; McGraw-Hill: New York, NY, USA, 1972; p. 713.
2. Lima, T.M.; Neves, C.A.R. *Sumário Mineral*; Departamento Nacional de Produção Mineral: Brasília, Brasil, 2016; Volume 35, pp. 78–79.
3. Vasconcelos, P.M. K-Ar and $^{40}\text{Ar}/^{39}\text{Ar}$ geochronology of weathering processes. *Annu. Rev. Earth Planet. Sci.* **1999**, *27*, 183–229. [[CrossRef](#)]
4. Dias, T.G.; Caxito, F. Recursos minerais de Minas Gerais—Manganês. *Recur. Min.* **2018**, *1*, 1–18.
5. IMnL-International Manganese Institute. About Manganese. Available online: <https://www.manganese.org/about-manganese/> (accessed on 19 August 2022).
6. Roy, S. Mineralogy of the different genetic types of manganese deposits. *Econ. Geol.* **1968**, *63*, 760–786. [[CrossRef](#)]
7. Biondi, J.C. *Processos Metalogenéticos e os Depósitos Minerais Brasileiros*, 1st ed.; Oficina de Textos: Curitiba, Brazil, 2003; pp. 378–423.
8. Robb, L. *Introduction to Ore-Formation Processes*, 1st ed.; Blackwell Science Ltd.: Melbourne, Australia, 2005; pp. 219–245.
9. Kämpf, N.; Curi, N.; Marques, J.J. Óxidos de alumínio, silício, manganês e titânio. In *Química e Mineralogia do solo*, 1st ed.; Melo, V.F., Alleoni, L.R.F., Eds.; Sociedade Brasileira de Ciência do Solo: Viçosa, Brasil, 2009; Volume 1, pp. 573–610.
10. Post, J.E. Manganese oxide minerals: Crystal structures and economic and environmental significance. *Proc. Natl. Acad. Sci. USA* **1999**, *96*, 3447–3454. [[CrossRef](#)]
11. Bernadini, S.; Bellatreccia, F.; Muncichia, A.C.; Ventura, G.D.; Sodo, A. Raman spectra of natural manganese oxides. *J. Raman Spectrosc.* **2019**, *50*, 873–888. [[CrossRef](#)]
12. Post, J.E.; McKeown, D.A.; Heaney, P.J. Raman spectroscopy study of manganese oxides: Tunnel structures. *Am. Miner.* **2020**, *105*, 1175–1190. [[CrossRef](#)]
13. Post, J.E.; McKeown, D.A.; Heaney, P.J. Raman spectroscopy study of manganese oxides: Layer structures. *Am. Miner.* **2021**, *106*, 351–366. [[CrossRef](#)]
14. Costa, M.R.M.; Silva, J.P.A.; Silva, R.D. *Sumário Mineral: Manganês*; Departamento Nacional de Produção Mineral: Brasília, Brasil, 2018; pp. 1–4.
15. Medeiros, K.A. *Anuário Mineral Brasileiro: Principais Substâncias Metálicas*; Agência Nacional de Mineração: Brasília, Brasil, 2022; pp. 1–35.
16. Pinheiro, W.F.; Filho, O.B.F.; Neves, C.A.R. *Anuário Mineral Brasileiro: Principais Substâncias Metálicas*; Agência Nacional de Mineração: Brasília, Brasil, 2017; pp. 1–43.
17. Veríssimo, C.U. Evolução Geológica dos Corpos de Protominério e Mineralizações de Manganês Associadas, Porção Leste de São Paulo e Sul de Minas Gerais. Master's Thesis, Universidade Estadual Paulista, Rio Claro, Brazil, 1991.
18. Fermor, L.L. The Manganese Ore Deposits of India. *Mem. Geol. Surv. India* **1909**, *37*, 272.
19. Hasui, Y. A grande colisão pré-cambriana do sudeste brasileiro e a estruturação regional. *Geociências* **2010**, *29*, 141–169.
20. Fuck, R.A.; Jardim de Sá, E.F.; Pimentel, M.M.; Dardenne, M.A.; Pedrosa-Soares, A.C. As faixas de dobramentos marginais do Cráton do São Francisco: Síntese dos conhecimentos. *O Cráton São Fr.* **1993**, *1*, 161–186.
21. Fuck, R.A.; Pimentel, M.M.; D'el-Rey Silva, L.J.H. Compartimentação tectônica na porção oriental da província Tocantins. In *Congresso Brasileiro de Geologia*; Balneário Camboriú: Santa Catarina, Brasil, 1994; Volume 1, p. 215.
22. Brito Neves, B.B.; Campos Neto, M.C.; Fuck, R.A. From Rodinia to western Gondwana: An approach to the Brasiliano-pan African cycle and orogenic collage. *Episodes* **1999**, *22*, 155–166. [[CrossRef](#)]
23. Campos Neto, M.C. Orogenic systems from southwestern Gondwana, an approach to Brazilian-pan African Cycle and orogenic collage in south-eastern Brazil. In *Tectonic Evolution of South America*; Cordani, U.G., Milani, E.J., Thomaz Filho, A., Campos, D.A., Eds.; Instituto de Geociências, Universidade de São Paulo: Rio de Janeiro, Brazil, 6–17 August 2000; pp. 335–365.
24. Trouw, R.A.J.; Nunes, R.P.M.; Castro, E.M.O.; Trouw, C.C.; Matos, G.C. Nota explicativa das Folhas Varginha (SF.23-V-D-VI) e Itajubá (SF.23-Y-B-III). *Prog. Geol. Bras.* **2008**, *1*, 1–99.
25. Pimentel, M.M.; Fuck, R.A. Neoproterozoic crustal accretion in central Brazil. *Geology* **1992**, *20*, 375–379. [[CrossRef](#)]
26. Campos Neto, M.C.; Basei, M.A.S. Evolução estrutural brasileira do nordeste de São Paulo: Dobramentos superpostos e esboço estratigráfico e tectônico. In *4º Simpósio Regional de Geologia*; Instituto de Geociências-Universidade de São Paulo: São Paulo, Brasil, 1983; pp. 61–78.
27. Campos Neto, M.C.; Basei, M.A.S.; Alves, F.R.; Vasconcelos, A.C.B. A nappe de cavalgamento de Socorro (SP-MG). In *33º Congresso Brasileiro de Geologia*; Rio de Janeiro, Brasil, 1984; Volume 4, pp. 1809–1822.

28. Campos Neto, M.C. Evolução do pré-cambriano paulista e regiões adjacentes. In *5° Simpósio Regional de Geologia*; São Paulo, Brasil, 1985; Volume 2, pp. 561–576.
29. Campos Neto, C.M.; Caby, R. Terrane accretion and upward extrusion of high pressure granulites in the Neoproterozoic nappes of Southeast Brazil: Petrological and structural constraints. *Tectonics* **2000**, *19*, 669–687. [[CrossRef](#)]
30. Janasi, V.; Alves, A.; Vlach, S.R.F.; Leite, R.J. Granitos peraluminosos da porção central da Faixa Ribeira, Estado de São Paulo: Sucessivos eventos de reciclagem da crosta continental no Neoproterozóico. *Geol. USP* **2003**, *3*, 13–24. [[CrossRef](#)]
31. Rocha, B.C.; Moraes, R.; Moller, A.; Cioffi, C.R.; Jercinovic, M.J. Timing of anatexis and melt crystallization in the Socorro–Guaxupé Nappe, SE Brazil: Insights from trace element composition of zircon, monazite and garnet coupled to U–Pb geochronology. *Lithos* **2017**, *277*, 337–355. [[CrossRef](#)]
32. Wernick, E. Contribuição à estratigrafia do Pré-Cambriano do leste do estado de São Paulo e áreas vizinhas. *Rev. Bras. Geoc.* **1978**, *8*, 206–216.
33. Zanardo, A. Pesquisa Geológica e de Matérias-Primas Cerâmicas do Centro Nordeste do Estado de São Paulo e Vizinhanças: Sistematização Crítica da Produção Técnico-Científica. Ph.D. Thesis, Universidade Estadual Paulista, Rio Claro, Brazil, 2003.
34. Ebert, H. Ocorrências de Fácies Granulíticas no Sul de Minas Gerais e áreas adjacentes. Em dependências das estruturas orogênicas: Hipóteses sobre sua origem. *Anais Acad. Bras. Ciênc.* **1968**, *40*, 215–229.
35. Cioffi, C.R.; Neto, M.D.C.C.; Moeller, A.; Rocha, B.C. Paleoproterozoic continental crust generation events at 2.15 and 2.08 Ga in the basement of the southern Brasília Orogen, SE Brazil. *Precambrian Res.* **2016**, *275*, 176–196. [[CrossRef](#)]
36. Felicissimo, J. Gondito no estado de São Paulo. *Instituto Geográfico e Geológico* **1939**, *25*, 93–125.
37. Pires, F.R.M.; Leonardos, O.H., Jr.; Parenti Couto, J.G. Gonditos na região de Pouso Alegre, Minas Gerais. *Mineração e Metalurgia* **1970**, *52*, 237–239.
38. Wernick, E.; Fernandes, N.A.; Almeida, N.F., Jr. Gonditos de Socorro e Itapira, SP. *Mineração e Metalurgia* **1976**, *39*, 16–21.
39. Angeli, N.; Khan, H.; Ito, G.M.; De Carvalho, S.G.; Jimenez-Rueda, J.R.; Penha, U.C. Geologia e caracterização tecnológica do minério de manganês da mina Córrego do Cocho, Itapira (SP). *Geologia USP* **2011**, *11*, 107–130. [[CrossRef](#)]
40. Ross, J.L.S. Relevo Brasileiro: Uma nova proposta de Classificação. *R. Depto. Geogr.* **1985**, *4*, 25–39. [[CrossRef](#)]
41. Brasil. *Projeto RADAMBRASIL—Folha SF-23 Vitória/Rio de Janeiro*; Ministério das Minas e Energia: Rio de Janeiro, Brazil, 1983.
42. Köeppen, W. Climatologia: Con un estudio de los climas de la tierra. *Fondo Cult. Econ.* **1948**, *1*, 478.
43. Reboita, M.S.; Rodrigues, M.; Silva, L.F.; Alves, M.A. Aspectos climáticos do estado de Minas Gerais. *Rev. Bras. Climat.* **2015**, *17*, 206–226.
44. Ávila, L.F.; Mello, C.R.D.; Viola, M.R. Mapeamento da precipitação mínima provável para o sul de Minas Gerais. *Bras. Eng. Agríc. Ambient. J.* **2009**, *13*, 906–915. [[CrossRef](#)]
45. Zancopé, M.H.C. Análise Morfodinâmica do rio Mogi Guaçu. Ph.D. Thesis, Universidade Estadual de Campinas, Campinas, Brazil, 2008.
46. Bacha, A.L.R.; Sardinha, D.S.; Godoy, L.H.; Ancelmi, M.F. Geoquímica de piroclastos intemperizados da Caldeira Vulcânica de Poços de Caldas, Minas Gerias. *Geol. USP* **2020**, *20*, 63–80.
47. Ramdohr, P. *The Ore Minerals and Their Intergrowths*, 2nd ed.; Pergamon Press: Berlin, Germany, 1980; Volume 2, pp. 1021–1045.
48. Costa, M.R.M.; Figueredo, R.C. *Balanço Mineral: Manganês*; Departamento Nacional de Produção Mineral: Brasília, Brasil, 2001; pp. 426–427.
49. Faria, G.L.D. Estudo da Intensidade de Crepitação de Minérios Granulados de Manganês do Brasil. Master’s Thesis, Universidade Federal de Ouro Preto (UFOP), Ouro Preto, Brazil, 2008.
50. Walde, D.H.G.; Gierth, E.; Leonardos, O.H. Stratigraphy and mineralogy of the manganese ores of Urucum, Mato Grosso, Brazil. *Geol. Rundsch.* **1981**, *70*, 1077–1085. [[CrossRef](#)]
51. Klein, C.; Ladeira, E.A. Geochemistry and mineralogy of Neoproterozoic banded iron-formations and some selected, siliceous manganese formations from the Urucum District, Mato Grosso do Sul, Brazil. *Econ. Geol.* **2004**, *99*, 1233–1244. [[CrossRef](#)]
52. Costa, M.L.D.; Fernandez, O.J.C.; Requelme, M.E.R. O depósito de manganês do Azul, Carajás: Estratigrafia, mineralogia, geoquímica e evolução geológica. In *Caracterização de Depósitos Minerais em Distritos Mineiros da Amazônia*; 2005; pp. 227–334.
53. Viana, N.C.S. Caracterização mineralógica dos litotipos de minério de manganês sílico-carbonatado da mina morro da mina. In *67° Congresso da Associação Brasileira de Metalurgia, Materiais e Mineração*; Rio de Janeiro, Brasil, 2012; pp. 214–221.
54. Faria, G.L.; Reis, E.L.; Araújo, F.G.S.; Vieira, C.B.; Júnior, N.J. Caracterização química, física e mineralógica do produto granulado de manganês proveniente da Mina de Urucum. In *XXIII Encontro Nacional de Tratamento de Minérios e Metalurgia Extrativa*; Gramado, Brazil, 2009; pp. 87–92.
55. Vasconcelos, P.M.; Becker, T.A.; Renne, P.R.; Brimhall, G.H. Direct dating of weathering phenomena by K–Ar and $^{40}\text{Ar}/^{39}\text{Ar}$ analysis of K–Mn oxides. *Geochim. Cosmochim. Acta* **1994**, *58*, 1635–1665. [[CrossRef](#)]
56. Ruffet, G.; Innocent, C.; Michard, A.; Feraud, G.; Beauvais, A.; Nahon, D.; Hamelin, B. A geochronological $^{40}\text{Ar}/^{39}\text{Ar}$ and $^{87}\text{Rb}/^{87}\text{Sr}$ study of K–Mn oxides from the weathering sequence of Azul, Brazil. *Geochim. Cosmochim. Acta* **1966**, *60*, 2219–2232. [[CrossRef](#)]
57. Spier, C.A.; Vasconcelos, P.M.; Oliveira, S.M.B. $^{40}\text{Ar}/^{39}\text{Ar}$ geochronological constraints on the evolution of lateritic iron deposits in the Quadrilátero Ferrífero, Minas Gerais, Brazil. *Chem. Geol.* **2006**, *234*, 79–104. [[CrossRef](#)]
58. Piacentini, T.; Vasconcelos, P.M.; Farley, K.A. $^{40}\text{Ar}/^{39}\text{Ar}$ constraints on the age and thermal history of the Urucum Neoproterozoic banded iron-formation, Brazil. *Precambrian Res.* **2013**, *228*, 48–62. [[CrossRef](#)]

59. Vasconcelos, P.M.; Farley, K.A.; Stone, J.; Piacentini, T.; Fifield, L.K. Stranded landscapes in the humid tropics: Earth's oldest land surface. *Earth Planet. Sci. Lett.* **2019**, *519*, 152–164. [[CrossRef](#)]
60. Meybeck, M. Global chemical weathering of surficial rocks estimated from river dissolved load. *Am. J. Sci.* **1987**, *287*, 401–428. [[CrossRef](#)]
61. Martini, I.P.; Chesworth, W. *Weathering, Soils and Paleosols*, 1st ed.; Elsevier Science Publications: Amsterdam, The Netherlands, 1992.
62. Pedro, G. Essai sur la caractérisation géochimique des différents processus zonaux résultant de l'altération des roches superficielles (cycle aluminosilicique). *Comptes Rendus Hebd. Seances Acad. Sci. Ser.* **1966**, *262*, 1828–1831.
63. Tardy, Y. Characterization of the principal weathering types by the geochemistry of waters from some European and African crystalline massifs. *Chem. Geol.* **1971**, *7*, 253–271. [[CrossRef](#)]
64. White, A.F.; Blum, A.E. Effects of climate on chemical weathering in watersheds. *Geochim. Cosmochim. Acta* **1995**, *59*, 1729–1747. [[CrossRef](#)]
65. Millot, R.; Gaillardet, J.; Dupré, B.; Allègre, C.J. The global control of silicate weathering rates and the coupling with physical erosion: New insights from rivers of the Canadian Shield. *Earth Planet. Sci. Lett.* **2002**, *196*, 83–98. [[CrossRef](#)]
66. Oliva, P.; Viers, J.; Dupré, B. Chemical weathering in granitic environments. *Chem. Geol.* **2003**, *202*, 225–256. [[CrossRef](#)]
67. West, A.J.; Galy, A.; Bickle, M. Tectonic and climatic controls on silicate weathering. *Earth Planet. Sci. Lett.* **2005**, *235*, 211–228. [[CrossRef](#)]
68. Dessert, C.; Dupré, B.; François, L.M.; Schott, J.; Gaillardet, J.; Chakrapani, G.; Bajpai, S. Erosion of Deccan Traps determined by river geochemistry: Impact on the global climate and the $^{87}\text{Sr}/^{86}\text{Sr}$ ratio of seawater. *Earth Planet. Sci. Lett.* **2001**, *188*, 459–474. [[CrossRef](#)]
69. Dessert, C.; Dupré, B.; Gaillardet, J.; François, L.M.; Allègre, C.J. Basalt weathering laws and the impact of basalt weathering on the global carbon cycle. *Chem. Geol.* **2003**, *202*, 257–273. [[CrossRef](#)]
70. Rimstidt, J.D. Quartz solubility at low temperatures. *Geochim. Cosmochim. Acta* **1997**, *61*, 2552–2558. [[CrossRef](#)]
71. Velbel, M.A. Natural weathering mechanisms of almandine garnet. *Geology* **1984**, *12*, 631–634. [[CrossRef](#)]
72. Hem, J.D. *Chemical Equilibria and Rates of Manganese Oxidation*; US Government Printing Office: Washington, DC, USA, 1963.
73. Vasconcelos, P.M.; Carmo, I.O. Calibrating denudation chronology through $^{40}\text{Ar}/^{39}\text{Ar}$ weathering geochronology. *Earth-Sci. R.* **2018**, *179*, 411–435. [[CrossRef](#)]
74. Carmo, I.O.; Vasconcelos, P.M. $^{40}\text{Ar}/^{39}\text{Ar}$ geochronology constraints on Late Miocene weathering rates in Minas Gerais, Brazil. *Earth Planet. Sci. Lett.* **2006**, *241*, 80–94. [[CrossRef](#)]
75. Hénoque, O.; Ruffet, G.; Colin, F.; Feraud, G. $^{40}\text{Ar}/^{39}\text{Ar}$ dating of West African lateritic cryptomelanes. *Geochim. Cosmochim. Acta* **1998**, *62*, 2739–2756. [[CrossRef](#)]
76. Dammer, D.; McDougall, I.; Chivas, A.R. Timing of weathering-induced alteration of manganese deposits in Western Australia: Evidence from K/Ar and $^{40}\text{Ar}/^{39}\text{Ar}$ dating. *Econ. Geol.* **1999**, *94*, 87–108. [[CrossRef](#)]
77. Bonnet, N.J.; Beauvais, A.; Arnaud, N.; Chardon, D.; Jayanada, J. Cenozoic lateritic weathering and erosion history of Peninsular India from $^{40}\text{Ar}/^{39}\text{Ar}$ dating of supergene K-Mn oxides. *Chem. Geol.* **2016**, *446*, 33–53. [[CrossRef](#)]
78. De Putter, T.; Ruffet, G.; Yans, J.; Mees, F. The age of supergene manganese deposits in Katanga and its implications for the Neogene evolution of the African Great Lakes Region. *Ore Geol. Rev.* **2015**, *71*, 350–362. [[CrossRef](#)]
79. De Putter, T.; Liégeois, J.; Dewaele, S.; Caiteux, J.; Mees, F. Paleoproterozoic manganese and base deposits at Kisenge-Kamata (Katanga, D.R. Congo). *Ore Geol. Rev.* **2018**, *96*, 181–200. [[CrossRef](#)]
80. Dekoninck, A.; Monié, P.; Blockmans, S.; Hatert, F.; Rochez, G.; Yans, J. Genesis and $^{40}\text{Ar}/^{39}\text{Ar}$ dating of K-Mn oxides from Stavelot Massif (Ardenne, Belgium): Insights into Oligocene to Pliocene weathering periods in Western Europe. *Ore Geol. Rev.* **2019**, *115*, 103191. [[CrossRef](#)]
81. De Putter, T.; Ruffet, G. Supergene manganese ore records 75 Myr-long Campanian to Pleistocene geodynamic evolution and weathering history of the Central African Great Lakes Region—Tectonics drives, climate assists. *Gondwana Res.* **2020**, *83*, 96–117. [[CrossRef](#)]
82. Pharoe, B.K.; Evdokimov, A.N.; Gembitskaya, I.M.; Bushuyev, Y.Y. Mineralogy, geochemistry and genesis of the post-Gondwana supergene manganese deposit of the Carletonville-Ventersdorp area, North West Province, South Africa. *Ore Geol. Rev.* **2020**, *120*, 103372. [[CrossRef](#)]
83. Conceição, F.T.; Bonotto, D.M. Use of U-isotopes disequilibrium to evaluate the weathering rates and fertilizer derived uranium at São Paulo State, Brazil. *Environ. Geol.* **2003**, *44*, 408–418. [[CrossRef](#)]
84. Conceição, F.T.; Bonotto, D.M. Weathering rates and anthropogenic influences in a sedimentary basin, São Paulo State, Brazil. *Appl. Geochem.* **2004**, *19*, 575–591. [[CrossRef](#)]
85. Conceição, F.T.; Sardinha, D.S.; Souza, A.D.G.; Bonito, D.M. Hydrochemical relationship at Meio Stream watershed (Leme city), São Paulo State, Brazil. *Rev. Bras. Geoc.* **2007**, *37*, 389–400.
86. Sardinha, D.S.; Conceição, F.T.; Bonotto, D.M.; Salles, M.H.F.; Angelucci, V.A. Avaliação do balanço anual de cátions e ânions na bacia do Alto Sorocaba (SP). *Rev. Bras. Geoc.* **2008**, *38*, 730–740. [[CrossRef](#)]
87. Conceição, F.T.; Sardinha, D.S.; Souza, A.D.G.; Navarro, G.R.B. Anthropogenic influences on annual flux of cations and anions at Meio Stream basin, São Paulo State, Brazil. *Water Air Soil Pollut.* **2010**, *205*, 79–91. [[CrossRef](#)]

88. Sardinha, D.S.; Bonotto, D.M.; Conceição, F.T. Weathering rates at Alto Sorocaba basin, Brazil, using U-isotopes and major cations. *Environ. Earth Sci.* **2010**, *61*, 1025–1036. [[CrossRef](#)]
89. Sardinha, D.S.; Bonotto, D.M.; Godoy, L.H.; Conceição, F.T.; Moreno, M.M.T. Denudação química e implicações na qualidade das águas superficiais da bacia do Rio Jaú (SP). *Rev. Bras. Geoc.* **2012**, *13*, 337–349.
90. Conceição, F.T.; Santos, C.M.; Sardinha, D.S.; Navarro, G.R.B.; Godoy, L.H. Chemical weathering rate, denudation rate, and atmospheric and soil CO₂ consumption of Paraná flood basalts in São Paulo state, Brazil. *Geomorphology* **2015**, *233*, 41–51. [[CrossRef](#)]
91. Couto Júnior, A.A.; Conceição, F.T.; Fernandes, A.M.; Cunha, C.M.L.; Spatti Júnior, E.P. Geoquímica fluvial aplicada à avaliação das taxas de intemperismo químico e remoção de solo da Formação Rio Claro. *Ver. Bras. Geomorfol.* **2016**, *17*, 451–464. [[CrossRef](#)]
92. Fernandes, A.M.; Conceição, F.T.; Spatti Junior, E.P.; Sardinha, D.S.; Mortatti, J. Chemical weathering rates and atmospheric/soil CO₂ consumption of igneous and metamorphic rocks under tropical climate in southeastern Brazil. *Chem. Geol.* **2016**, *443*, 54–66. [[CrossRef](#)]
93. Sardinha, D.S.; Godoy, L.H.; Conceição, C.T. Taxa de intemperismo e consumo de CO₂ em relevo cuestasiforme com substrato basáltico e arenítico no estado de São Paulo. *Geol. USP* **2019**, *19*, 117–134. [[CrossRef](#)]
94. Spatti Júnior, E.P.; Conceição, F.T.; Fernandes, A.M.; Sardinha, D.S.; Moruzzi, R.B. Chemical weathering rates of clastic sedimentary rocks from the Paraná Basin in the Paulista Peripheral Depression, Brazil. *J. South Am. Earth Sci.* **2019**, *96*, 102–369. [[CrossRef](#)]
95. Fernandes, A.M.; Conceição, F.T.; Spatti Júnior, E.P.; Couto Júnior, A.A.; Hissler, C.; Mortatti, J. Human influences on the present denudation rates of the Paulista Peripheral Depression, Brazil. *Geomorphology* **2020**, *351*, 106–955. [[CrossRef](#)]
96. Conceição, F.T.; Vasconcelos, P.M.; Godoy, L.H.; Navarro, G.R.B.; Montibeller, C.C.; Sardinha, D.S. Water/rock interactions, chemical weathering and erosion, and supergene enrichment in the Tapira and Catalão I alkaline-carbonatite complexes, Brazil. *J. Geochem. Explor.* **2022**, *237*, 106–999. [[CrossRef](#)]
97. Meneguel, E.C.; Conceição, F.T.; Navarro, G.R.B.; Christofolletti, S.R.; Mota, J.F.M. Chemical weathering processes generating the raw material used in porcelain stoneware industry in the São Paulo State, Brazil. *J. South Am. Earth Sci.* **2022**, *118*, 103–926. [[CrossRef](#)]
98. Ling, F.T.; Post, J.E.; Heaney, P.J.; Santelli, C.M.; Ilton, E.S.; Burgos, W.D.; Rose, A.W. A multi-method characterization of natural terrestrial birnessites. *Am. Miner.* **2020**, *105*, 833–847. [[CrossRef](#)]

Disclaimer/Publisher’s Note: The statements, opinions and data contained in all publications are solely those of the individual author(s) and contributor(s) and not of MDPI and/or the editor(s). MDPI and/or the editor(s) disclaim responsibility for any injury to people or property resulting from any ideas, methods, instructions or products referred to in the content.